Advanced Materials
Research and Technology

https://www.techsync.com

Van der Waals interactions and their impacts on the Raman spectra in two-dimensional layered atomic crystals

Jia-An Yan

Department of Physics, Astronomy, and Geosciences, Towson University
8000 York Road, Towson, MD 21252, USA
Email: jiaanyan@gmail.com

ABSTRACT: Van der Waals (vdW) interactions in seven typical two-dimensional (2D) bilayer crystals, including bilayer graphene, MoS_2, WS_2, phosphorene, $TaSe_2$, SnSe, and WS_2/MoS_2 heterostructure are examined by first-principles calculations. While the local density approximation (LDA) predicts a wide variety of binding energies ranging from 9 meV/Å² in bilayer graphene to 34 meV/Å² in bilayer SnSe, calculations with vdW corrections at the vdW-DF2 level yield a universal binding energy: ~19 meV/Å², in close agreement with previous report. A detailed analysis of the charge density redistribution induced by the interlayer coupling reveals a dramatic difference predicted from LDA and vdW-DF2 among these layered systems, which span from semiconductors, semimetals to metals. Finally, effects of interlayer coupling on the electronic and vibrational properties of recently fabricated WS_2/MoS_2 heterostructure are discussed.

KEYWORDS: VAN DER WAALS INTERACTIONS; RAMAN SPECTRA; TWO-DIMENSIONAL LAYERED CRYSTALS; FIRST-PRINCIPLES CALCULATIONS; HETEROSTRUCTURES.

1. Introduction

Van der Waals (vdW) interactions, first proposed in real gases and liquids by van der Waals in 1873 [1], are ubiquitous in biological, chemical and condensed matter systems [2-7]. This long-range attractive interaction arises from instantaneous dipoles induced by quantum charge fluctuations around nucleus on each chemical species [2, 3], and plays a crucial role in many phenomena such as protein folding. Thanks to the recent developments on both theoretical methods [8-13] and experimental techniques [14], vdW interactions receive explosive attention in recent years [14-19], and its study spans almost all areas of natural sciences [2-7].

The advent of graphene [20-23] and other two-dimensional (2D) layered materials [24-26] has opened an era for exploring vast potentials of 2D materials. In these so-called vdW systems, including few-layer graphene [22], transition metal dichalcogenides (TMDs) [27-29], few-layer phosphorus [30-32], and SnSe [33], the vdW interaction provides a decisive force to stabilize the crystal structure along the stacking direction. Owing to this weak interlayer coupling, it is now possible to choose and stack atomic layers of arbitrary compositions to build desired layered heterostructures [34-37], which would be otherwise impossible to synthesize via other known methods. Heterostructures such as BN/graphene [38-41], MoS_2/graphene [42, 43], and WS_2/MoS_2 [44, 45] have been successfully demonstrated in experiments, which exhibit remarkable electronic and optical properties [36, 44-46]. While vdW interaction has been widely studied in the past decades, insights into this force are still limited, particularly in 2D layered atomic crystals [48-50]. A thorough understanding of the vdW interactions among nanomaterials will form a crucial step towards the design of vdW-based 2D materials for diverse applications. The large variety of 2D atomic crystals, on the other hand, offers a versatile platform to study fundamental vdW interaction itself in condensed matter physics [17].

In response to the rapid progress in 2D material research, we present here a first-principles study of the vdW interactions in seven typical bilayer crystals, including bilayer graphene (BLG), MoS_2, WS_2, $TaSe_2$, bilayer phosphorene (BLP) [47], SnSe, and WS_2/MoS_2 heterostructure, as shown in Fig. 1. For each bilayer crystal, we consider the most stable structure that has been theoretically predicted in literature and/or observed in experiments. For example, bilayer MoS_2 will follow the stacking geometry of bulk 2H-MoS_2 (c.f. Fig. 1(e)), and bilayer graphene will be AB-stacked (c.f. Fig. 1(a)), etc. Note that the selected systems have shown great potentials for diverse applications, and exhibited a wide range of electronic properties, including semimetals (BLG), metals ($TaSe_2$), and semiconductors (BLP, MoS_2, WS_2, WS_2/MoS_2, and SnSe).

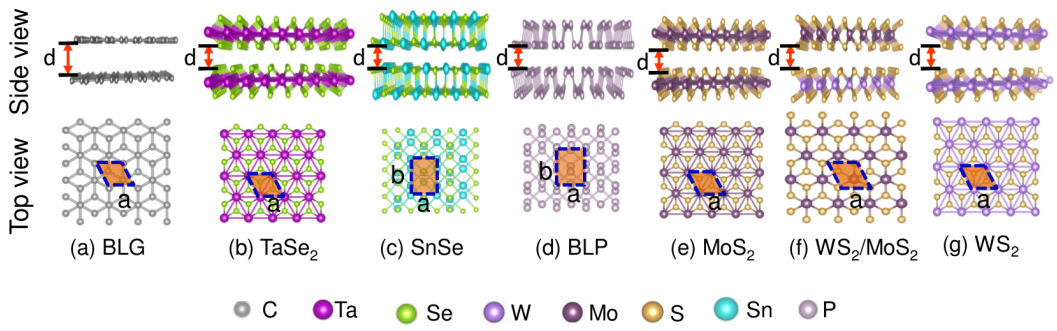

Figure 1. Atomic structures for all the seven bilayer crystals considered in this work. The interlayer separation d, the lattice parameters a and b are indicated on the top view of each lattice. The area of the unit cell for each crystal is shaded. Note that d is defined as the thickness of the vacuum region between two layers, not the usual interlayer distance. Among the seven crystals, (c) and (d) possess rectangular unit cell, while all others are hexagonal lattice. Upper row: side view; Lower row: top view.

The binding energy E_b, which is defined as the energy needed to separate the two layers from the equilibrium separation to an infinite distance, is a key quantity for the discussion of vdW interactions and the layer-related properties, e.g., the exfoliation energy, stacking fault energy, and surface energy. Graziano et al. [48] have reported improved implementations of vdW-functionals applied for studying 2D compounds such as BN, graphene, and several TMDs. Björkman et al. [49] reported a universal binding energy of about 20 meV/Å^2 in several 2D

crystals. His recent work [50] further studied the performance of vdW functionals in predicting the structural parameters in layered crystals. In this work, we will address the following remaining questions: 1) How does the binding energy change in other semiconducting systems such as black phosphorous and SnSe? 2) What is the charge density redistribution induced by the interlayer coupling? And 3) how does the vdW corrections affect the electronic band structure and vibrational properties? We study E_b in the above mentioned 2D materials and reveal the common nature of the vdW interaction in these crystals. We will then discuss effects of interlayer coupling on the electronic and vibrational properties of WS_2/MoS_2 heterostructure. The knowledge from this study will advance the design of 2D heterostructures using various constituent 2D layers, and further provide clues for probing the weak vdW interactions.

The paper is organized as follows. In Section II, we briefly present the calculation details. In Section III, the results will be discussed. A summary will be given in Section IV.

2. Calculation Details

Our ab initio calculations are performed using the VASP code [51, 52] at three different levels: local density approximation (LDA), generalized-gradient approximation (GGA) with PBE [53], and PBE with vdW-DF2 corrections [10-12]. The cutoffenergy in the plane wave expansion is 500 eV. A Monkhorst-Pack uniform k-grid of 36×36×1 is employed for metallic BLG and $TaSe_2$, while a shifted 12×12×1 k-grid are used for semiconducting bilayer crystals such as MoS_2. A vacuum region of more than 30 Å is introduced along the out-of-plane (z) direction to eliminate spurious interactions among periodic images. The optimization of both the lattice parameters and atomic positions have been performed unless the stress is less than 1 kB and the forces on atoms are less than 0.02 eV/Å. All the self-consistent calculations are converged until the energy change is within 1×10^{-6} eV. For the vibrational properties and Raman spectra, we employ the Quantum Espresso (QE) code [54].

The seven bilayer crystals considered here have different number of atoms in the unit cell, ranging from 4 atoms in BLG, 6 atoms in MoS_2 and WS_2, to 8 atoms in BLP and SnSe (see Fig. 1 for the unit cells). In addition, most of these crystals possess sublayer structure. For example, monolayer MoS_2 actually has S-Mo-S trilayer structure. To compare the binding energy on an equal footing, one could use energy per atom or energy per unit area. Here, we calculate E_b in two different forms: one is the "raw" energy E_b^T - the binding energy per unit cell, and the other is the binding energy per unit area of the 2D lattice $E_b^A = E_b^T/A$, with A the 2D area of the unit cell. As will be seen below, the results of E_b^A reveal a common nature of vdW interactions in all of these 2D materials, in agreement with previous work [49].

3. Results and Discussions

The evolutions of the total energy per unit cell, calculated from LDA, GGA, and vdW-DF2, are presented as a function of interlayer separation d on the upper row of Fig. 2, respectively. The corresponding total energy per unit area are shown on the lower row in Fig. 2. In all cases, the energy at d > 8 Å is nearly constant, and therefore establishes a reference point, which has been shifted to zero. From Fig. 2, one can see that all the E-d curves exhibit a similar trend: the total energy reaches minimum at the equilibrium separation $d = d_0$; it increases dramatically to be repulsive when the separation decreases $d < d_0$; when $d > d_0$, the energy slowly increases to a constant value, approaching the energy of two isolated monolayers. The trend of the E-d curves is similar to the famous Lennard-Jones (LJ) potential $E_{LJ} = A/r^{12} - B/r^6$, with the second term describing the instantaneous dipole-dipole interaction.

By determining the difference between minima and the reference point, the binding energy E_b can be calculated, as schematically indicated for SnSe in Fig. 2(a) and 2(b), respectively. All the calculated results have been summarized in Table I.

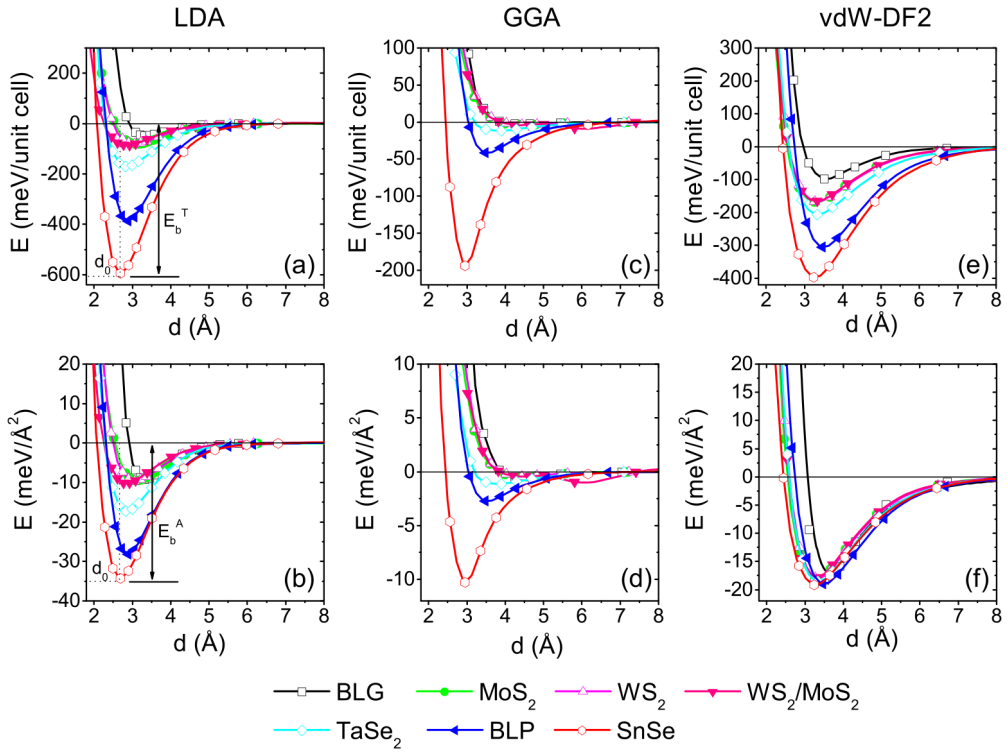

Figure 2. Evolution of total energy as a function of the interlayer separation d calculated from LDA (first column), GGA (middle column) and vdW-DF2 (third column). (a), (c), and (e) show the total energy per unit cell as a function of d. (b), (d) and (f) show the total energy per unit area as a function of d. Note that the total energy at the d > 8 Å has been set as a reference. As an example, the binding energies E_b^T and E_b^A at equilibrium separation d0 are explicitly indicated for the SnSe in (a) and (b), respectively.

We focus on the E_b^A as listed in the last column of Table I, inferred from Fig. 2(b), 2(d) and 2(f). The LDA predicts a wide range of E_b^A in 2D materials, from 9 meV/Å² in BLG to 34 meV/Å² for SnSe. The metallic charge-density wave material $TaSe_2$ has a E_b^A of 17 meV/Å². Clearly, the LDA results could be categorized into three different coupling regimes: strong, intermediate, and weak. The strong vdW binding occurs for tin monochalcogenide and black phosphorene, with E_b^A almost four times the value in BLG. This is mainly due to the much smaller interlayer separation d calculated from LDA. The intermediate regime includes $TaSe_2$, which is only half of that of SnSe. The weak regime includes semimetallic graphene and semiconducting TMDs, such as MoS_2, WS_2 and their heterostructure, roughly ~10 meV/Å². On the other hand, GGA predicts a somewhat similar behavior, as shown in Fig. 2(d), but the absolute values are significantly smaller. For SnSe, the binding energy is only ~10 meV/Å², about 1/3 of the LDA value, while BLG has only 0.5 meV/Å². The result of TaSe2 falls in between.

In contrast, the vdW-DF2 shows a dramatically different behavior. Although Fig. 2(e) presents a wide range of absolute values from 97 meV/unit cell in BLG to 397 meV/unit cell for SnSe, the E_b^A reveals a surprisingly universal binding energy in all of these 2D materials, as shown in Fig. 2(f). Specifically, all of these E_b^A falls between 18~19 meV/Å². These results can be identified more clearly from the column bar plot in Fig. 3(a).

The calculated E_b^A are in good agreement with previous work [49]. Table I also lists the available binding energies within random-phase approximation (RPA) from [50]. The RPA data are believed to be the most accurate theoretical values and are used as benchmarks for evaluating the performance of vdW exchange-functionals [11, 48, 50]. Our calculations show very good agreement with the RPA results, as can be seen from Table I. The universal binding energy is also consistent with the equilibrium separation d, as schematically shown in Fig. 3(b), which falls into a small range of 3.2~3.5 Å.

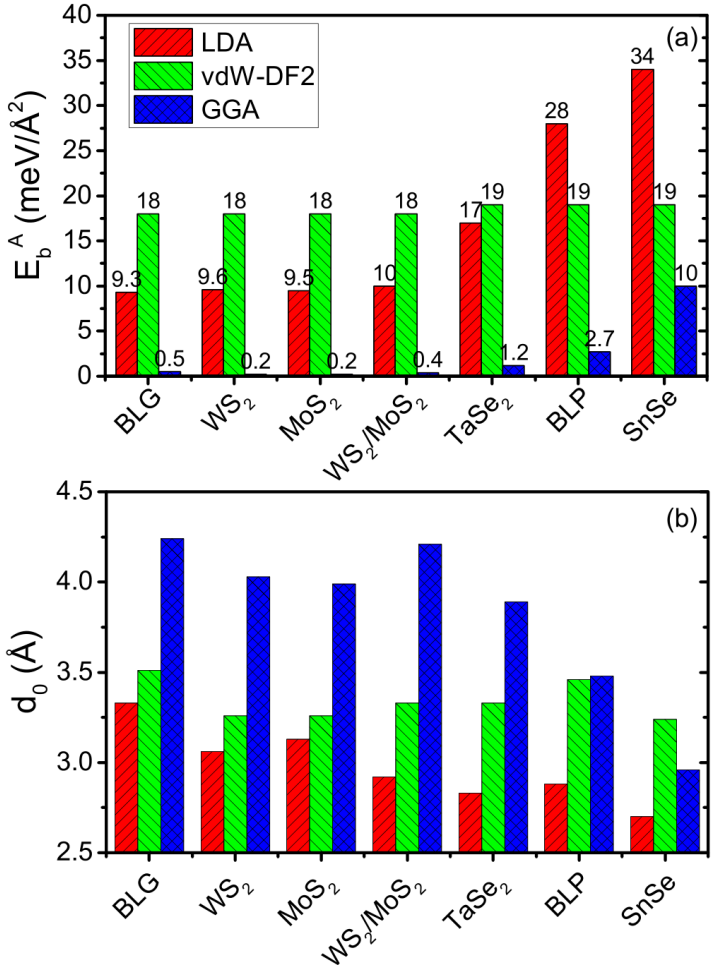

Figure 3. Column bar diagram of (a) the binding energy E_b^A and (b) the equilibrium separation d0 as listed in Table 1.

Table I also lists the obtained structure parameters. Three general observations emerge immediately: (1) In each crystal, LDA yields smallest lattice parameters, while GGA predicts the largest. The results from vdW-DF2, on the other hand, fall in between. This is particularly evident for the area of the unit cell A. (2) The equilibrium separations d predicted in LDA are significantly smaller than those of GGA and vdW-DF2. For example, in BLG, LDA predicts d_0 = 3.326 Å, about 28% and 5.6% smaller than the values of GGA (4.245 Å) and vdW-DF2 (3.513 Å). In all crystals except SnSe, the vdW-DF2 compromises results of LDA and GGA. (3) In SnSe, the vdW-DF2 predicts a significantly larger d_0 = 3.245 Å: 17% larger than the LDA value (2.698 Å), and even 8.7% larger than the GGA value (2.96 Å).

Table 1. The exchange-correlation (XC) functional, the calculated lattice parameter(s) a (b), the unit cell area A (Å²) of the unit cell, the equilibrium interlayer separation d_0 (Å), the binding energies E_b^T (meV/unit cell) and E_b^A (meV/Å²) for each bilayer system. The values shown in parenthesis are the RPA results from Ref. [50].

System	xc	a (b)	A	d_0	E_b^T	E_b^A
BLG	LDA	2.448	5.19	3.326	48	9.3
	GGA	2.468	5.27	4.245	2.6	0.49
	vdW-DF2	2.477	5.31	3.513	97	18.3 (18.3)
WS_2	LDA	3.107	8.36	3.060	80	9.6
	GGA	3.181	8.76	4.033	1.92	0.22
	vdW-DF2	3.278	9.31	3.264	167	17.9 (20.2)
MoS_2	LDA	3.136	8.52	3.131	81	9.5
	GGA	3.183	8.77	3.990	2.0	0.23
	vdW-DF2	3.284	9.34	3.261	169	18.1 (20.5)
WS_2/MoS_2	LDA	3.122	8.44	2.922	86	10.2
	GGA	3.181	8.76	4.214	3.4	0.39
	vdW-DF2	3.280	9.32	3.333	166	17.8
TaSe2	LDA	3.378	9.88	2.826	170	17.2
	GGA	3.467	10.41	3.891	12.0	1.15
	vdW-DF2	3.578	11.09	3.331	206	18.6 (19.4)
BLP	LDA	3.261, 4.211	13.73	2.882	387	28.2
	GGA	3.303, 4.590	15.161	3.477	41.4	2.73
	vdW-DF2	3.384, 4.752	16.08	3.463	306	19.0
SnSe	LDA	4.104, 4.220	17.32	2.698	594	34.3
	GGA	4.256, 4.453	18.95	2.96	194	10.2
	vdW-DF2	4.393, 4.723	20.75	3.245	397	19.1

We would like to remark that the binding energy in vdW materials also depends on the stacking geometry. For example, the AA-stacked bilayer graphene is calculated to be E_b^A = 16 meV/Å², slightly smaller than the AB-stacked BLG. We expect that other stacking order such as twisted bilayer graphene would fall in between these two limiting cases.

Why does the LDA predict distinct binding energy from vdW-DF2? To clarify the origin, we examine the charge density redistribution induced by the interlayer coupling. The charge density difference, $\Delta\rho$, is defined as $\Delta\rho = \rho_t - \rho_l - \rho_u$, with ρ_t, ρ_l, and ρ_u the charge densities of bilayer, lower layer and upper layer, respectively. All the charge densities are calculated using the same supercell and parameters. Hence, a positive $\Delta\rho$ indicates charge accumulation, while a negative $\Delta\rho$ implies charge depletion induced by weak interlayer coupling. The results have been shown for each crystal in Fig. 4. We find that in LDA, there will always be a charge accumulation between the two layers. This is particularly evident in BLG, as shown on the first row in Fig. 4. From BLG to SnSe (see the left column in Fig. 4), the charge redistribution of LDA becomes not so evident. Nevertheless, overall there is a charge overlap from LDA. This is understandable, since DFT will always predict a ground state with "bonding" between two layers. As a result, LDA predicts a smaller interlayer separation.

In contrast, the vdW-DF2 shows a completely opposite behavior of the charge density difference $\Delta\rho$: charge density is depleted between two layers because of the interlayer coupling, as shown

on the right column of Fig. 4. This is particularly evident in BLG and MoS_2. Overall, there is a charge depletion between two layers within vdW-DF2.

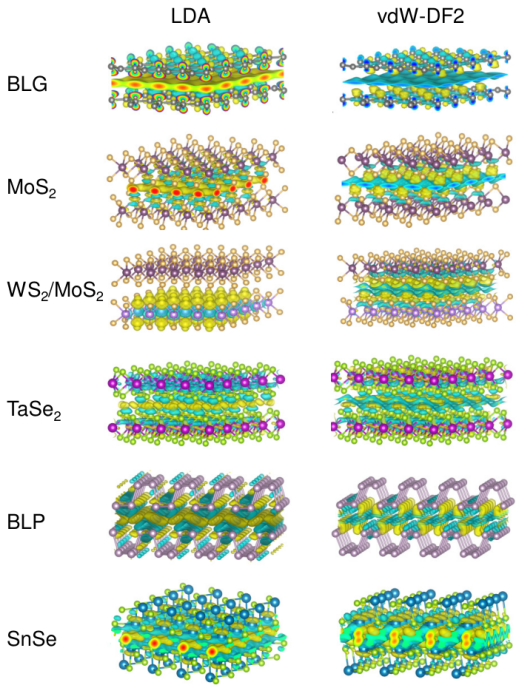

Figure 4. Isosurface of charge density difference Δρ. Yellow denotes charge accumulation while cyan green denotes charge depletion. The isosurface level is at approximately $\pm 1\times10^{-4}$ e/Å^3 for most systems.

VdW Heterostructures have attracted a lot of attention in recent years [37]. Here we focus on the results of WS_2/MoS_2 heterostructure. From Fig. 4, LDA yields an unusual charge redistribution for WS_2/MoS_2 heterostructure as compared with other bilayer crystals: Only the bottom WS_2 layer shows a visible charge redistribution under the influence of the upper MoS_2 layer, while little charge density difference occurs on the upper MoS_2 layer. This result is distinct from the result of vdW-DF2, in which a significant charge redistribution takes place on both WS_2 and MoS_2 layers.

Fig. 5(a) shows the electronic band dispersions of WS_2/MoS_2 heterostructure along the high symmetric Γ-K-M-Γ direction in both LDA and vdW-DF2. Within LDA, there is an indirect band gap of about 1.4 eV, while the vdW-DF2 lowers the conduction band near K by more than 0.6 eV. Consequently, the indirect band gap in vdW-DF2 becomes only 0.8 eV. Besides the structural parameters and binding energies, the vdW corrections induce remarkable effects on the valence band and conduction bands in this 2D heterostructures.

On the other hand, vdW interactions seem to have very small effects on the vibrational properties. The Raman spectra of WS_2/MoS_2 are simply the combination of constituent monolayer MoS_2 and WS_2. In Fig. 5(b), we show the LDA results of the Raman spectra of monolayer MoS_2, monolayer WS_2, and WS_2/MoS_2 heterostructure, respectively. The Raman peaks in WS_2/MoS_2 are located at 353.7, 384.8, 404.3, and 417.0 cm^{-1}, a clear combination of Raman peaks of individual layers. Specifically, the modes at 384.8 and 404.3 cm^{-1} correspond to the E' (383.5 cm^{-1}) and A'1 (403.1 cm^{-1}) modes in monolayer MoS_2, respectively, while the modes at 353.7 and 417.0 cm^{-1} originate from those from WS_2 (356.8 and 417.5 cm^{-1}, respectively). Unnoticeable shift on the order of 1

cm^{-1} is observed. Our calculations are in good agreement with experimental data [45]. Despite the overestimation of the binding energy in WS_2/MoS_2, LDA seems to predict surprisingly accurate vibrational properties in this vdW heterostructure.

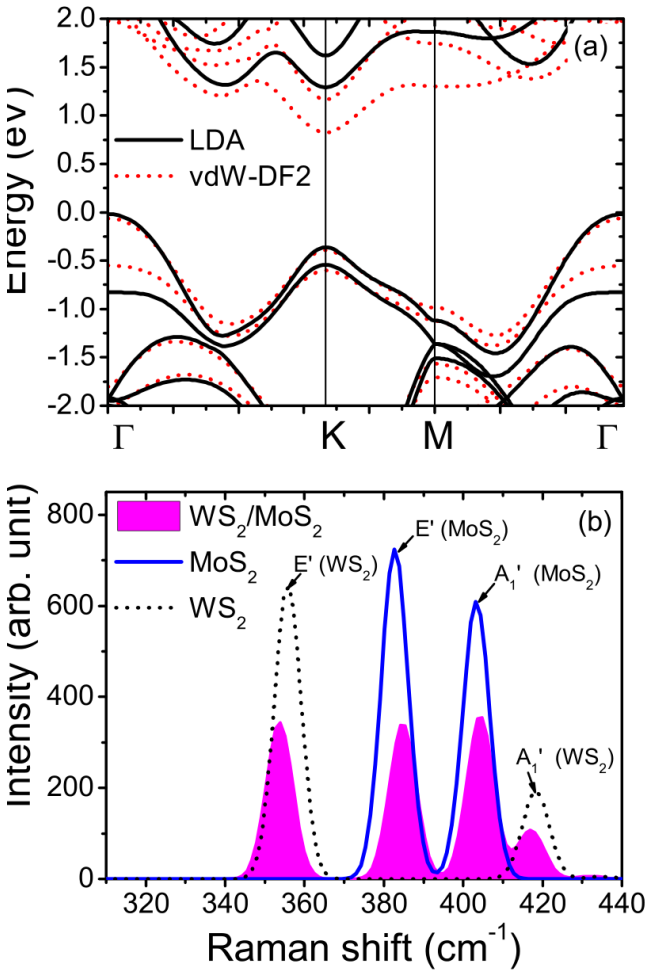

Figure 5. (a) Band structure of WS_2/MoS_2 heterostructure calculated with LDA (black solid) and vdW-DF2 (red dashed). The valence band maximum (VBM) at Γ has been shifted to zero. (b) The calculated Raman spectra of monolayer WS_2 (black dashed), MoS_2 (blue solid) and WS_2/MoS_2 heterostructure (pink shaded). The peak positions of Raman-active E' and A'1 modes in monolayer MoS_2 and WS_2 have been indicated, respectively.

4. Summary

In summary, we present a first-principles study of the vdW interactions in 2D materials. While LDA predicts a wide range of binding energies, the advanced calculations at the vdW-DF2 level yield a universal value of ~19 meV/Å², revealing a common nature of all these 2D systems. In addition, analysis of charge density difference shows a dramatic difference between LDA and vdW-DF2: Within LDA, there is a significant charge accumulation between two layers, while a charge depletion occurs with vdW-DF2. Furthermore, the vdW-DF2 exhibits a remarkable reduction on the indirect band gap in WS_2/MoS_2 heterostructure, implying an evident effect of interlayer vdW coupling on the electronic properties in this system. In contrast, the vibrational

properties seem insensitive to the vdW interactions: The Raman spectra of WS_2/MoS_2 heterostructure are simply the combination of those from individual layers, in good agreement with experimental observation.

It has been generally believed that LDA will overestimate the vdW bonding in layered crystals, while GGA significantly underestimates it. However, as can be seen from Table I, the LDA E_b^A of in BLG, MoS_2, WS_2, and WS_2/MoS_2 are roughly 50% of those calculated with vdW-DF2. In TaSe2, the LDA result is close to that of vdW-DF2. Only in BLP and SnSe the LDA yields significant larger binding energy than vdW-DF2.

We would like to emphasize that the origin of the dispersion forces - nonlocal electron-electron correlations - makes their accurate theoretical description very challenging. This is especially true for DFT where local or semilocal functionals lack the necessary ingredients to describe the nonlocal effects [11, 15, 19]. In fact, developing methods that include dispersion, at least approximately, has been one of the most important fields of development in DFT in the last decade [19]. Although the vdW-DF2 has been proven to be very successful in many systems, further experimental work is needed to verify the validity of this correction in 2D crystals.

On the other hand, the versatile combinations of various 2D materials provide an important platform for studying the fundamental nature of the vdW interactions both theoretically and experimentally. In contrast to the molecular systems and other biological systems, 2D materials might provide a relatively convenient system to fabricate, measure and study the vdW interactions. Our results call on further experimental work on the fundamental nature of vdW interactions in 2D materials.

Acknowledgments

The author thanks Paul Kent for useful discussions. This work is supported by the Seed Fund from OSPR at the Towson University. This work used the Extreme Science and Engineering Discovery Environment (XSEDE) Carver, Comet and Expanse at the SDSC through allocation TG-DMR160101.

References

[1] J. D. van der Waals. On the gaseous and the liquid state (University of Leiden, The Netherlands), Dissertation, 1873.

[2] D. Langbein. Theory of van der Waals Attraction (Springer, Berlin, 1974).

[3] G. C. Maitland, M. Rigby, E. B. Smith, W. A. Wakeham. Intermolecular Forces, Their Origin and Determination (Clarendon Press, Oxford), 1981.

[4] Carel J. Van Oss , Manoj K. Chaudhury , Robert J. Good. Interfacial Lifshitz-van der Waals and polar interactions in macroscopic systems. Chem. Rev. 88, 927-941 (1988).

[5] A. D. Buckingham, P. W. Fowler, J. M. Hudson. Theoretical studies of van der Waals molecules and intermolecular forces. Chem. Rev. 88, 963-988 (1988).

[6] A. J. Stone. The Theory of Intermolecular Forces (Clarendon Press, Oxford), 1996.

[7] I. G. Kaplan. Intermolecular Interactions: Physical Picture, Computational Methods and Model Potentials (John Wiley and Sons Ltd, England), 2006.

[8] M. Dion, H. Rydberg, E. Schröder, D. C. Langreth, and B. I. Lundqvist. Van der Waals Density Functional for General Geometries. Phys. Rev. Lett. 92, 246401 (2004).

[9] G. Román-Pérez and J. M. Soler. Efficient Implementation of a van der Waals Density Functional: Application to Double-Wall Carbon Nanotubes. Phys. Rev. Lett. 103, 096102 (2009).

[10] J. Klimes, D.R. Bowler, A. Michelides. Chemical accuracy for the van der Waals density functional. J. Phys.: Cond Matt. 22, 022201 (2010).

[11] J. Klimes, D.R. Bowler, A. Michelides. Van der Waals density functionals applied to solids. Phys. Rev. B. 83, 195131 (2011) and references therein.

[12] K. Lee, E. D. Murray, L. Kong, B. I. Lundqvist, and D. C. Langreth. Higher-accuracy van der Waals density functional. Phys. Rev. B 82, 081101(R) (2010).

[13] Kristian Berland et al. van der Waals forces in density functional theory: a review of the vdW-DF method. Rep. Prog. Phys. 78 066501 (2015).

[14] C. Wagner et al. Non-additivity of molecule-surface van der Waals potentials from force measurements. Nat. Commun. 5, 5568 (2014).

[15] Jianmin Tao, John P. Perdew, and Adrienn Ruzsinszky. Accurate van der Waals coefficients from density functional theory. Proc. Nat. Acad. Soc. USA. 109, 18-21 (2012).

[16] V. V. Gobre and A. Tkatchenko. Scaling laws for van der Waals interactions in nanostructured materials. Nat. Commun. 4, 2341 (2013).

[17] Anand Sharma, Peter Harnish, Alexander Sylvester, Valeri N. Kotov, and A. H. Castro Neto. van der Waals forces and electron-electron interactions in two strained graphene layers. Phys. Rev. B 89, 235425 (2014).

[18] W. Gao and A. Tkatchenko. Sliding mechanisms in multilayered hexagonal boron nitride and graphene: The effects of directionality, thickness and sliding constraints. Phys. Rev. Lett. 114, 096101 (2015).

[19] A. Tkatchenko. Current understanding of van der Waals effects in realistic materials. Adv. Funct. Mater. 25, 2054-2061 (2015).

[20] K. S. Novoselov, et al. Two-dimensional atomic crystals. Proc. Natl Acad. Sci. USA 102,10451-10453 (2005).

[21] A. K. Geim and K. S. Novoselov. The rise of graphene. Nat. Mater. 6, 183 (2007).

[22] A. K. Geim. Graphene: Status and Prospects. Science 324, 1530-1534 (2009).

[23] K. S. Novoselov, V. I. Fal'ko, L. Colombo, P. R. Gellert, M. G. Schwab, and K. A. Kim. Roadmap for graphene. Nature 490, 192-200 (2012).

[24] R. Mas-Ballesté, C. Gómez-Navarro, J. Gómez-Herrero and F. Zamora. 2D materials: to graphene and beyond. Nanoscale 3, 20-30 (2011).

[25] M. Xu, T. Lian, M. Shi, and H. Chen. Graphene-like two-dimensional materials. Chem. Rev. 113, 3766-3798 (2013).

[26] S. Z. Butler et al. Progress, challenges, and opportunities in two-dimensional materials beyond graphene. ACS Nano 7, 2898-2926 (2013).

[27] K. F. Mak, C. Lee, J. Hone, J. Shan, and T. F. Heinz. Atomically thin MoS_2: a new direct-gap semiconductor. Phys. Rev. Lett. 105, 136805 (2010).

[28] B. Radisavljevic, A. Radenovic, J. Brivio, V. Giacometti, and A. Kis. Single-layer MoS_2 transistors. Nature Nanotechnol. 6, 147-150 (2011).

[29] Q. H. Wang, K. Kalantar-Zadeh, A. Kis, J. N. Coleman, and M. S. Strano. Electronics and optoelectronics of two-dimensional transition metal dichalcogenides. Nat. Nanotechnol. 7, 699-712 (2012).

[30] Likai Li, Yijun Yu, Guo Jun Ye, Qingqin Ge, Xuedong Ou, Hua Wu, Donglai Feng, Xian Hui Chen and Yuanbo Zhang. Black phosphorus field-effect transistors. Nat. Nanotechnol. 9, 372-377 (2014) doi:10.1038/nnano.2014.35

[31] Jingsi Qiao, Xianghua Kong, Zhi-Xin Hu, Feng Yang and Wei Ji. High-mobility transport anisotropy and linear dichroism in few-layer black phosphorus. Nat. Commun. 5, 4475 doi:10.1038/ncomms5475.

[32] Andres Castellanos-Gomez et al. Isolation and characterization of few-layer black phosphorus. 2D Mater. 1, 025001 (2014). doi:10.1088/2053-1583/1/2/025001.

[33] L. D. Zhao,S. H. Lo, Y. Zhang, H. Sun, G. Tan, C. Uher, C. Wolverton, V. P. Dravid, M. G. Kanatzidis. Ultralow thermal conductivity and high thermoelectric figure of merit in SnSe crystals. Nature 508, 373-377 (2014). doi:10.1038/nature13184

[34] Guanhui Gao, Wei Gao, E. Cannuccia, Jaime Taha-Tijerina, Luis Balicas, Akshay Mathkar, T. N. Narayanan, Zhen Liu, Bipin K. Gupta, Juan Peng, Yansheng Yin, Angel Rubio and Pulickel M. Ajayan. Artificially Stacked Atomic Layers: Toward New van der Waals Solids. Nano Lett. 12, 3518-3525 (2012).

[35] M. Osada, and T. Sasaki. Two-dimensional dielectric nanosheets: novel nanoelectronics from nanocrystal building blocks. Adv. Mater. 24, 210-228 (2012).

[36] L. Britnell et al. Field-effect tunneling transistor based on vertical graphene heterostructures. Science 335, 947-950 (2012).

[37] A. K. Geim and I. V. Grigorieva. Van der Waals heterostructures. Nature 499, 419-425 (2013), doi:10.1038/nature12385.

[38] Z. Liu et al. Direct growth of graphene/hexagonal boron nitride stacked layers. Nano Lett. 11, 2032-2037 (2011).

[39] M. S. Bresnehan et al. Integration of hexagonal boron nitride with quasi-freestanding epitaxial graphene: toward waferscale, high-performance devices. ACS Nano 6, 5234-5241 (2012).

[40] J. M. Garcia et al. Graphene growth on h-BN by molecular beam epitaxy. Solid Stat. Comm. 152 975-978 (2012).

[41] C. R. Dean et al. Graphene based heterostructures. Solid Stat. Comm. 152, 1275-1282 (2012).

[42] S. Bertolazzi, D. Krasnozhon, and A. Kis. Nonvolatile memory cells based on MoS_2/graphene heterostructures. ACS Nano 7, 3246-3252 (2013).

[43] T. Georgiou et al. Vertical field-effect transistor based on graphene- MoS_2 heterostructures for flexible and transparent electronics. Nature Nanotechnol. 8, 100-103 (2013).

[44] K. Kosmider and J. Fernández-Rossier. Electronic properties of the MoS_2- WS_2 heterojunction. Phys. Rev. B 87, 075451 (2013).

[45] Y. Gong et al. Vertical and in-plane heterostructures from WS_2/MoS_2 monolayers. Nat. Mater. 13, 1135-1142 (2014).

[46] B. Hunt et al. Massive Dirac fermions and Hofstadter butterfly in a van der Waals heterostructure. Science 10.1126/science.1237240 (2013).

[47] J. Dai and X. C. Zeng. Bilayer phosphorene: Effect of stacking order on bandgap and its potential applications in thin-film solar cells. J. Phys. Chem. Lett. 5, 1289-1293 (2014).

[48] G. Graziano, J. Klimes, F. Fernandez-Alonso, and A. Michaelides. Improved description of soft layered materials with van der Waals density functional theory. J. Phys.: Condens. Matter 24, 424216 (2012).

[49] T. Björkman, A. Gulans, A. V. Krasheninnikov, and R. M. Nieminen. van der Waals Bonding in Layered Compounds from Advanced Density-Functional First-Principles Calculations. Phys. Rev. Lett. 108, 235502 (2012).

[50] T. Björkman. Testing several recent van der Waals density functionals for layered structures. J. Chem. Phys. 141, 074708 (2014); doi: 10.1063/1.4893329.

[51] G. Kresse and J. Furthmüller. Efficiency of ab-initio total energy calculations for metals and semiconductors using a plane-wave basis set. Comput. Mat. Sci. 6, 15-50 (1996).

[52] G. Kresse and J. Furthmüller. Efficient iterative schemes for ab initio total-energy calculations using a plane-wave basis set. Phys. Rev. B 54, 11169 (1996).

[53] J. P. Perdew, K. Burke, and M. Ernzerhof. Generalized Gradient Approximation Made Simple. Phys. Rev. Lett. 77, 3865 (1996)

[54] Giannozzi, P. et al. QUANTUM ESPRESSO: a modular and open-source software project for quantum simulations of materials. J. Phys. Condens. Matter 21, 395502 (2009).